The Meteoritical Society

Meteoritics & Planetary Science 42, Nr 1, 113–130 (2007)
Abstract available online at http://meteoritics.org

L-chondrite asteroid breakup tied to Ordovician meteorite shower by multiple isochron ^{40}Ar-^{39}Ar dating

Ekaterina V. KOROCHANTSEVA[1, 2], Mario TRIELOFF[1*], Cyrill A. LORENZ[2], Alexey I. BUYKIN[1, 2], Marina A. IVANOVA[2], Winfried H. SCHWARZ[1], Jens HOPP[1], and Elmar K. JESSBERGER[3]

[1]Mineralogisches Institut, Ruprecht-Karls-Universität Heidelberg, Im Neuenheimer Feld 236, D-69120 Heidelberg, Germany
[2]Vernadsky Institute of Geochemistry, Kosygin Street 19, 119991 Moscow, Russia
[3]Institut für Planetologie, Westfälische Wilhelms-Universität, Wilhelm-Klemm-Str. 10, D 48149 Münster, Germany
[*]Corresponding author. E-mail: trieloff@min.uni-heidelberg.de

(Received 22 June 2006; revision accepted 05 November 2006)

Abstract–Radiochronometry of L chondritic meteorites yields a rough age estimate for a major collision in the asteroid belt about 500 Myr ago. Fossil meteorites from Sweden indicate a highly increased influx of extraterrestrial matter in the Middle Ordovician ~480 Myr ago. An association with the L-chondrite parent body event was suggested, but a definite link is precluded by the lack of more precise radiometric ages. Suggested ages range between 450 ± 30 Myr and 520 ± 60 Myr, and can neither convincingly prove a single breakup event, nor constrain the delivery times of meteorites from the asteroid belt to Earth. Here we report the discovery of multiple ^{40}Ar-^{39}Ar isochrons in shocked L chondrites, particularly the regolith breccia Ghubara, that allow the separation of radiogenic argon from multiple excess argon components. This approach, applied to several L chondrites, yields an improved age value that indicates a single asteroid breakup event at 470 ± 6 Myr, fully consistent with a refined age estimate of the Middle Ordovician meteorite shower at 467.3 ± 1.6 Myr (according to *A Geologic Time Scale 2004*). Our results link these fossil meteorites directly to the L-chondrite asteroid destruction, rapidly transferred from the asteroid belt. The increased terrestrial meteorite influx most likely involved larger projectiles that contributed to an increase in the terrestrial cratering rate, which implies severe environmental stress.

INTRODUCTION

Most meteorites originate from small bodies in the asteroid belt that formed about 4.6 billion years ago in the course of planet formation around the young Sun. Unlike the larger terrestrial planets, these small bodies cooled rapidly without extended magmatic activity. Indeed, many meteorites have high radiometric ages very close to the formation age of the solar system, some of them recording undisturbed cooling after parent-body heating (Pellas et al. 1997; Trieloff et al. 2003a). However, many other meteorites show disturbed radiometric ages caused by secondary collisional evolution that ultimately led to the destruction of their asteroidal parent body, and eventually to their transfer to Earth as meter-size bodies. Prominent examples are HED meteorites from asteroid Vesta (Bogard and Garrison 2003; Kunz et al. 1995; Korochantseva et al. 2005). L chondrites are the major meteorite class that shows the most frequently disturbed radiometric clocks and shock effects (e.g., planar deformation features in olivine, maskelynite transformation of plagioclase, melt veins and pockets; see Stöffler et al. 1991), indicating a major collision or asteroid breakup about 500 Myr ago (Heymann 1967; Turner 1969; Bogard et al. 1976, 1995; Bogard and Hirsch 1980; Kaneoka et al. 1988; McConville et al. 1988; Kunz et al. 1997). The discovery of fossil meteorites in Middle Ordovician limestone (~480 Myr old), with chemical compositions of chromite similar to L or LL chondrites, led to a tentative association to the L-chondrite asteroid breakup event (Schmitz et al. 1997, 2001, 2003). This event was first assigned by U, Th-He chronology to 520 ± 60 Myr ago (Heymann 1967), but this value was questioned and 340 ± 50 Myr was suggested as the "true" age for the L-asteroid event (Alexeev 1998), which would then make it virtually unconnected to the Ordovician meteorite stream. As U, Th-He chronometry is susceptible to various influences, e.g., cosmogenic ^{4}He or secondary loss of ^{4}He, it is possible that the low age estimate is due to secondary disturbances by impacts following (and occluding) the 500 Myr event.

These problems may be circumvented by using the K-Ar chronometer, as it is less susceptible to perturbations. However, respective age estimates are also divergent and/or relatively imprecise, ranging from 450 ± 30 Myr (McConville et al. 1988) to 500–600 Myr (Turner 1969; Bogard et al. 1976, 1995; Bogard and Hirsch 1980). These studies showed that the main problem in ^{40}Ar-^{39}Ar chronology is incomplete resetting of the K-Ar system, i.e., incomplete degassing of inherited radiogenic ^{40}Ar. Instead of broad age plateaus (i.e., segments of constant age), at best only partial plateaus were obtained that comprised only up to three gas extractions. Bogard et al. (1995) argued that impact melts from L chondrite Chico yielded unrealistically high values of ~530 Myr, thereby questioning the reliability of impact melts in providing precise impact ages. Turner (1969) determined ^{40}Ar-^{39}Ar ages based on low temperature extractions of Barratta and Ergheo of 470 ± 50 Myr and 530 ± 10 Myr, respectively. Values as high as 530 Myr for the L chondrite parent body event would only allow a link to ~480 Myr old fossil Ordovician meteorites if the collisional fragments needed tens of millions of years for transfer from the asteroid belt. However, this is excluded by short cosmic-ray exposure ages of <1 Myr for the fossil chondrites (Heck et al. 2004). All in all, a more precise age value for L-chondrite parent body event is essential: should it predate the fossil meteorites by, e.g., more than 10 Myr, this would imply that these two events were virtually unconnected.

SAMPLES AND EXPERIMENTAL PROCEDURES

We analyzed the L5 chondrite Ghubara (Binns 1968; Ferko et al. 2002). Polished thin sections of Ghubara (~3.5 cm^2, ~90 mm^2) were examined using traditional methods of optical microscopy in transmitted and reflected light. Mineral compositions were determined with the CAMEBAX Microbeam at the Vernadsky Institute, Moscow. The analyses were performed at 15 keV accelerating voltage, 20 nA beam current, and 20 s counting time.

^{40}Ar-^{39}Ar analysis followed standard procedures (Trieloff et al. 1994, 1997; Jessberger et al. 1980; Schwarz and Lippolt 2002). Ghubara samples were wrapped in high-purity (99.999%) aluminum foil and irradiated in evacuated quartz ampoules at the GKSS-reactor in Geesthacht, Germany. In contrast to previous studies in which we attempted to enhance ^{38}Ar production from Cl by omission of Cd shielding (Trieloff et al. 2003b), we here suppressed the ^{37}Cl(n,γβ$^-$)^{38}Ar reaction by applying 1 mm cadmium shielding. Two neutron irradiations were performed. Irradiation #1 was performed with Ghubara xenolith (208.2 mg for 27 days, J value of 1.52 × 10^{-2}), and irradiation #2 was performed with Ghubara melt (25.0 mg for 18.5 days, J value of 0.80 × 10^{-2}). The flux monitors were 2.66 Gyr old NL25 hornblende (Schaeffer and Schaeffer 1977). Correction factors for interfering isotopes determined by CaF_2 monitors for both irradiations were $(^{36}Ar/^{37}Ar)_{Ca}$ = (4.6 ± 0.1) × 10^{-4}, $(^{38}Ar/^{37}Ar)_{Ca}$ = (8.8 ± 0.2) × 10^{-5}, $(^{39}Ar/^{37}Ar)_{Ca}$ = (9.6 ± 0.1) × 10^{-4}. For both irradiations, $(^{38}Ar/^{39}Ar)_K$ was (1.88 ± 0.13) × 10^{-2} and $(^{38}Ar/^{39}Ar)_K$ = (2.3 ± 0.23) × 10^{-3}, determined via a degassed sanidine glass. $(^{40}Ar/^{37}Ar)_{Ca}$ = (3 ± 3) × 10^{-3} was taken from Turner (1971) and $(^{40}Ar/^{39}Ar)_K$ = (1.23 ± 0.24) × 10^{-2} from Brereton (1970). The samples were stepwise heated to temperatures from 350 °C to 1700 °C (>30 temperature steps) using an induction-heated furnace (Ghubara melt) with ^{40}Ar blank values of 5 × 10^{-10}ccSTP at 900 °C and 34 × 10^{-10}ccSTP at 1400 °C (10 min heating duration) and a resistance-heated furnace (Ghubara xenolith) with ^{40}Ar blank values of <10^{-12}ccSTP at 1400 °C (10 min heating duration).

Apparent ages were calculated using the Steiger and Jäger (1977) conventions. For detailed Ar isotope data tables, see the Appendix. Plateau ages X and their uncertainties σ were calculated from n individual "plateau" extractions with age x_i and error σ_i. They are error weighted with $w_i = 1/\sigma_i^2$, i.e., the plateau age is $X = \Sigma(x_i\, w_i)/\Sigma w_i$ and the uncertainty is $\sigma = (\Sigma w_i(x_i - X)^2/(n-1)\Sigma w_i)^{1/2}$, or $\sigma = (1/\Sigma w_i)^{1/2}$ (the larger value is taken as uncertainty).

MINERALOGY OF GHUBARA

Ghubara (L5) has a shock stage of S4, according to the classification by Stöffler et al. (1991). The shock features include planar fractures and mosaicism in olivine, melt pockets, interconnecting melt veins, and opaque shock veins. Ghubara has a low weathering grade of W1. A large xenolith, about 1.5 cm^2 in size, stands out well against the main meteorite. Unlike the Ghubara main mass, which is black, the xenolith is light gray in color and has clear boundaries with the host meteorite. It is characterized by a chondritic texture, low weathering grade (W1), and slightly lower degree of shock metamorphism than the Ghubara host, although it is still classified as S4. The xenolith contains small opaque veins in silicate material and melt pockets. Mosaic extinction of olivines is not very intensive. Chondrules are of different types (microporphyritic olivine and olivine-pyroxene, barred olivine, radial pyroxene, and very rare cryptocrystalline). In the xenolith, the chondrule/matrix ratio is slightly higher than in the Ghubara host. Mineral chemistry of the xenolith (Table 1) shows that it belongs to ordinary chondrites of chemical group L and petrological type 5. Olivine is homogeneous. Pyroxenes are low-Ca orthopyroxenes and high-Ca augite, almost diopside. Accessories are FeNi metal grains, kamacite (Co 0.8 wt%), and troilite. Mesostasis of chondrules is typical of the Ghubara meteorite and has Na-rich plagioclase composition (Table 1). Another achondritic melt inclusion from Ghubara (Fig. 1) is a 1 × 0.4 cm macroscopically light green elliptic xenolith, sharply contacting with the chondrite host. The inclusion is composed of medium-grained (40–100 μm) subhedral olivine (50 vol%) and anhedral pyroxene grains (45 vol%). The chemical

Table 1. Chemical composition of main minerals from Ghubara melt and xenolith by electron microprobe (average and variations, wt%).

	SiO_2	TiO_2	Al_2O_3	Cr_2O_3	FeO[a]	MnO	MgO	CaO	Na_2O	K_2O	Total	En/Ab/Fo	Wo/An	Fs/Or/Fa
Ghubara melt														
Feldspathic glass	67.8	0.53	20.0	0.08	1.08		0.40	1.60	6.03	2.40	99.9	71.0	10.4	18.6
n[b] = 10	65.7–69.1	0.29–1.36	19.3–20.9	0.02–0.34	0.65–1.98		0.16–1.51	0.94–4.09	5.57–6.69	1.42–3.73		64.0–74.9	6.5–25.0	10.3–28.2
Olivine	39.2	0.04	0.09	0.35	21.0	0.44	38.9	0.06			100.1	76.7		23.3
n = 12	37.8–40.1	b.d.[c]–0.09	0.04–0.53	b.d.–2.14	18.3–23.1	0.37–0.50	37.6–41.7	0.04–0.09				74.4–80.3		19.7–25.6
Pyroxene	55.5	0.07	0.49	0.77	13.4	0.48	27.8	1.74	0.14		100.4	75.5	3.4	21.1
n = 3	54.7–56.2	0.06–0.09	0.47–0.53	0.74–0.79	13.0–13.8	0.43–0.52	27.5–28.4	1.27–2.58	0.05–0.24			73.6–76.5	2.5–5.0	20.9–21.4
Ghubara xenolith														
Mesostasis	68.0		20.9	0.03	0.76		0.44	2.15	7.25	1.06	100.6	79.4	12.7	8.0
n = 6	63.0–70.5		20.1–22.5	0–0.09	0.57–1.00		0.21–0.91	1.35–4.68	5.87–8.52	0.37–1.57		72.3–84.6	8.9–25.3	2.4–13.5
Olivine	38.3		0.05	0.09	22.6	0.44	38.7	0.08			100.3	75.3		24.7
n = 7	37.8–38.8		0.02–0.10	0.03–0.25	22.0–23.1	0.39–0.49	38.2–39.3	0.06–0.14				74.8–75.7		24.3–25.2
Orthopyroxene	55.7	0.15	0.21	0.17	13.6	0.45	28.6	0.77			99.7	77.3	1.5	21.2
n = 4	54.9–56.5	0.11–0.24	0.1–0.28	0.15–0.18	13.2–14.6	0.42–0.48	28.1–29.2	0.68–0.81				76.2–78.0	1.3–1.6	20.5–22.5
Clinopyroxene	53.7	0.36	1.09	1.35	4.91	0.23	16.1	21.1	0.84		99.6	47.2	44.4	8.4
n = 2	53.4–53.9	0.35–0.37	1.05–1.12	1.05–1.64	4.63–5.18	0.22–0.23	15.9–16.3	21.0–21.2	0.74–0.94			46.8–47.6	44.3–44.5	7.9–8.9

[a]All Fe as FeO.

[b]*n* = number of analyses.

[c]b.d. = below detection.

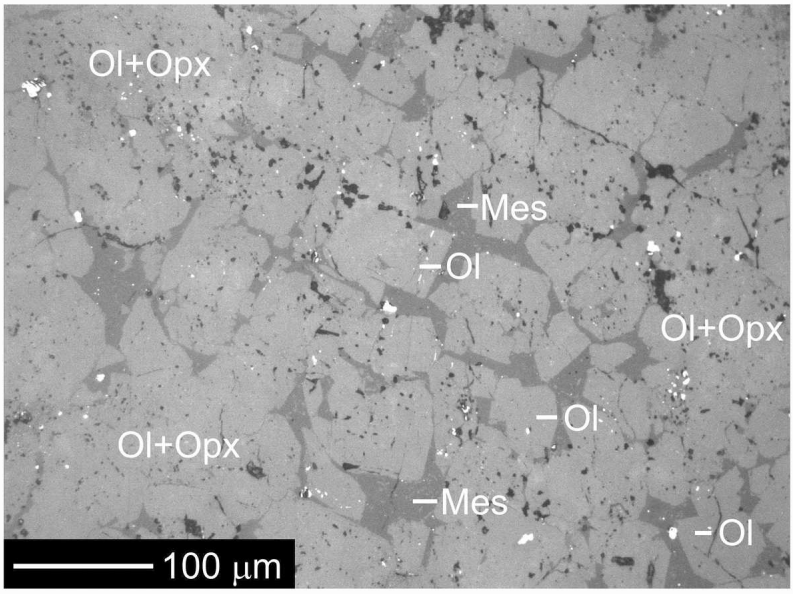

Fig. 1. A BSE image of Ghubara melt.

compositions of olivine and pyroxene grains are presented in Table 1 and are characterized by Fe/Mn of ~47 and ~28 (atomic), respectively. In a few places, olivine crystals are poikilitically enclosed within pyroxene. The compositions of silicates correspond to the host chondrite. The modal abundance of FeNi metal and troilite is <0.1 vol%. The interstitial spaces of silicates are filled with cryptocrystalline mesostasis of feldspathic composition (Table 1), containing rare inclusions of troilite, FeNi metal (Ni 8.8–15.3 wt%, Ni/Co = 12–29), and chromite. Troilite also forms tiny eutectic-like intergrowths with FeNi metal within tiny droplets. Chromite has a significant V content (V_2O_3 ~0.7 wt%). The metal is poor in Si, P, and S. When compared to the xenolith, the melt inclusion is significantly enriched in K, as commonly observed for chondritic melts (Kunz et al. 1997; Bogard et al. 1995).

For a more detailed mineralogical description (and experimental details) of the other L chondrites for which we reanalyzed isochrons and age spectra, we refer to the original study by Kunz et al. (1997) and references therein.

L CHONDRITE ^{40}Ar-^{39}Ar DATING

Figures 2a, 2b, 3a, and 3b display inverse isochrons and age spectra of the melt inclusion and the chondritic light xenolith, respectively. The melt age spectrum is highly irregular, if a conventional correction with an almost negligible amount of trapped primordial argon [$(^{40}Ar/^{36}Ar)_{trap}$ = 1 ± 1] is applied (Fig. 3a). It displays a saddle-shaped feature similar to terrestrial rocks containing excess argon. Surprisingly, the isochron plot (Fig. 2a) displays two distinct arrays, indicating two mixtures of in situ radiogenic argon and trapped argon with ratios of $(^{40}Ar/^{36}Ar)_{trap}$ = 303 ± 4 (presumably slightly altered terrestrial atmospheric argon) and 235.8 ± 1.6 (nonterrestrial). Correcting the age spectrum for these two distinct trapped components results in an age plateau comprising 23 temperature extractions (~95% ^{39}Ar release) with an age of 465 ± 6 Myr. The Ghubara xenolith yields an age spectrum (Fig. 3b) with apparent ages exceeding the age of the solar system, clearly indicative of redistributed excess argon rather than inherited (not mobilized) argon. The isochron analyses (Fig. 2b) yield another two components with $(^{40}Ar/^{36}Ar)_{trap}$ = 250 ± 10 and ~174/178, respectively (see Fig. A2 in the Appendix), resulting in an age spectrum with a plateau-like structure of 445 ± 24 Myr age. While this is not as precise as the melt sample, it highlights the possibility that even for age spectra highly contaminated by excess argon, this component can be identified and resolved from in situ radiogenic argon. This is, to our knowledge, the first report of (nonterrestrial) excess argon in asteroidal meteoritic samples identified and corrected for by a multiple isochron approach, which was also successfully applied to terrestrial samples in exceptional cases (Heizler and Harrison 1988; Trieloff et al. 1998; Hayatsu and Palmer 1975).

We note here that three circumstances favored our discovery. First, Ghubara is a regolith breccia with a high proportion of trapped solar gases that obviously equilibrated with remobilized inherited radiogenic argon 465 ± 6 Myr ago upon impact disruption of the asteroid. Second, we applied Cd shielding of the samples during neutron irradiation and chose a relatively short irradiation time (J = 0.008, see experimental procedures). These measures suppressed ^{38}Ar production from Cl via the $^{37}Cl(n,\gamma\beta^-)^{38}Ar$ reaction driven by thermal neutrons, allowing for a precise component resolution of cosmogenic ^{36}Ar, ^{38}Ar (produced in the last 15–20 Myr during cosmic ray exposure) and trapped ^{36}Ar, ^{38}Ar (see Appendix). Third, we

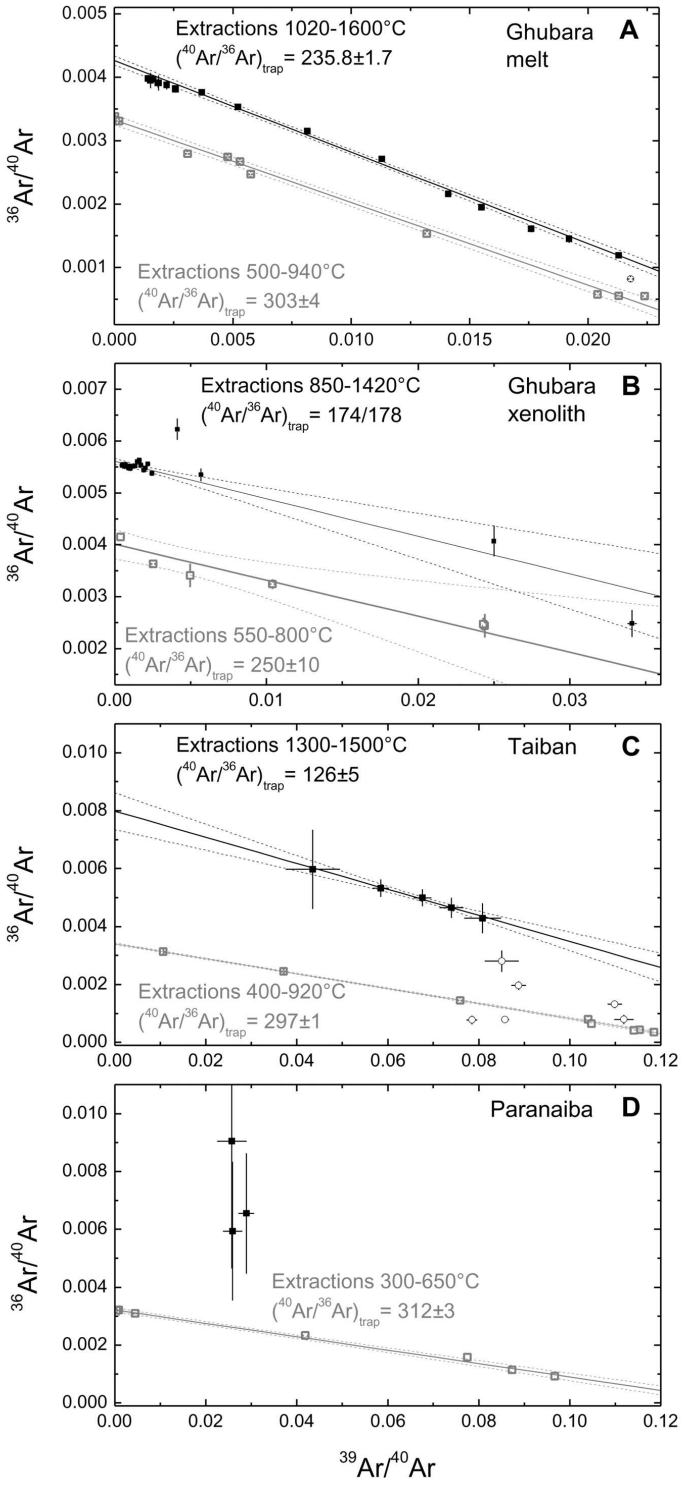

Fig. 2. Multiple isochrons in inverse isochrons plots of Ghubara melt (a), the Ghubara xenolith (b), Taiban (c), and Paranaiba (d). Only trapped ^{36}Ar is used to construct (inverse) isochrons, which requires proper separation from cosmogenic ^{36}Ar using ^{36}Ar/^{38}Ar ratios (see main text and the Appendix), e.g., by suppressing ^{38}Ar production from Cl. Most samples contain a trapped component with ^{40}Ar/^{36}Ar ratios similar or slightly higher than air (=295.5), degassing at low temperatures and probably related to weathering products. At high temperatures, most samples release an extraterrestrial trapped argon component with ^{40}Ar/^{36}Ar ratios < 295.5, most probably originating by equilibrating primordial (e.g., solar) argon with very low and previously accumulated argon with very high ^{40}Ar/^{36}Ar ratios. Argon carrier phases of trapped argon are not exactly known, while carrier phases of in situ radiogenic ^{40}Ar are the K-bearing phases feldspar or its impact-related derivatives (maskelynite, glass veins/melt pockets, occasionally hollandite structured). Dashed lines are confidence bands.

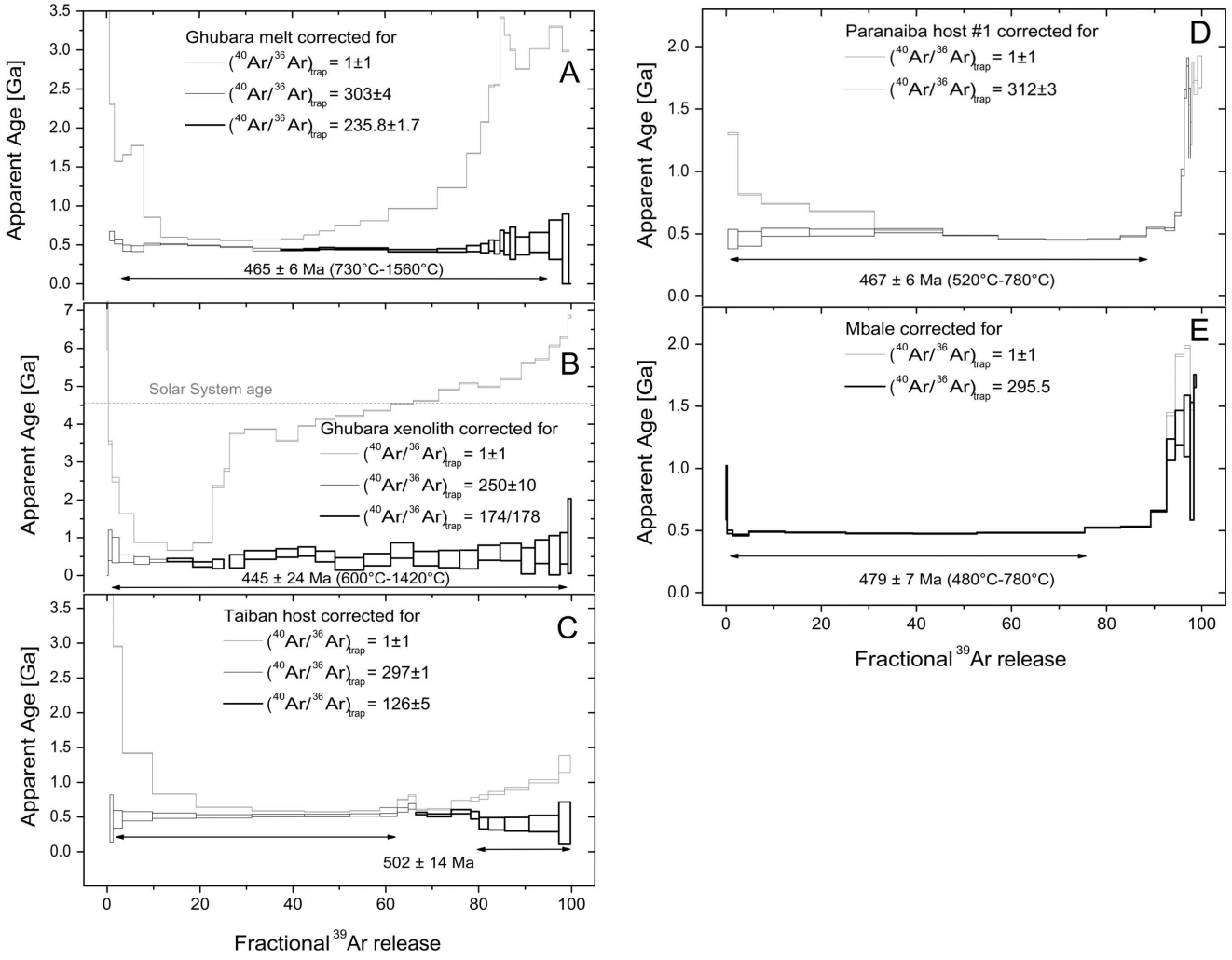

Fig. 3. Age spectra of Ghubara melt (a), Ghubara xenolith (b), Taiban (c), Paranaiba (d), and Mbale (e). Correction of the age spectra for the trapped argon components identified in inverse isochrons plot (Fig. 1) transforms highly irregular and implausible age spectra (with some apparent ages exceeding the age of the solar system) into plateau-like age spectra that all yield indistinguishable age values. Part of the remaining scatter in apparent ages within individual age spectra may be due to ^{39}Ar recoil (Turner and Cadogan 1974; Huneke and Smith, 1976). Our approach removes previous ambiguities in the age of the L-chondrite parent body breakup, yielding a highly concordant value (Table 2, text).

performed high-resolution analyses using about 30 temperature steps. This enabled us to construct proper isochrons with trapped ^{36}Ar, a prerequisite for isochron analyses. Our Ghubara results encouraged us to search for multiple isochrons in previously tabulated L-chondrite ^{40}Ar-^{39}Ar data sets (Bogard et al. 1995; Bogard and Hirsch 1980; McConville et al. 1988; Kunz et al. 1997). However, for two Peace River samples (McConville et al. 1988) and five Chico samples, trapped ^{36}Ar could not be identified (i.e., all samples had ^{36}Ar/^{38}Ar ratios <0.65). For Farmington and Louisville (Bogard and Hirsch 1980), Point of Rocks, and three further Chico samples (Bogard et al. 1995), trapped ^{36}Ar was restricted to ≤3 argon extractions. Wickenburg and Orvinio had six extractions with trapped argon, but not in the medium temperature steps that were characterized by >500 Myr excess ages (Bogard and Hirsch 1980). Only a few samples from the Heidelberg ^{40}Ar-^{39}Ar laboratories (Kunz et al. 1997) allowed construction of isochrons with a significant number of points (Figs. 2c and 2d; Table 2). However, in these cases effects of interference by Cl-derived ^{38}Ar could be larger than for Ghubara melt. Corrected age spectra are shown in Figs. 3c, 3d, and 3e. Taiban (L6) shows two arrays yielding two partial plateaus with an age of 502 ± 14 Myr; Paranaiba (L6) yields a nearly complete plateau of 467 ± 6 Myr. Many extractions belonging to this plateau do not contain trapped argon and are independent of such a correction. This is also the case for all plateau fractions of Mbale (L5–6) yielding an age of 479 ± 7 Myr. The corrected Bluff (L6) spectrum yield—similar to that of the Ghubara xenolith—a less precise plateau value of 491 ± 31 Myr (Fig. A2).

Table 2. ^{40}Ar-^{39}Ar age dating results of L chondrites. Listed are all L chondrites from this and previous studies for which an isochron approach[a] yielded age plateaus between 70 and 100% of the ^{39}Ar release and between 8 and 23 gas extractions. Mbale is added because it is the only L chondrite that shows a broad plateau without isochron correction.

L chondrite	Temperature range (°C)	No. of extractions	$(^{40}Ar/^{36}Ar)_{trapped}$ for correction	Plateau age[b] (Myr)	^{39}Ar release (%)	K-Ar age (Myr)	$^{36}Ar_{trapped}$ (10^{-8}ccSTP/g)	Extractions with $^{36}Ar_{trapped}$ (no./total)
Ghubara (L5) melt	730–940	6	303 ± 4	465 ± 6		1760	15.0	31/31
	1020–1560	17	235.8 ± 1.7		95			
Ghubara (L5) xenolith	600–750	4	250 ± 10			4350	17.5	29/29
	850–1420	19	174/178	445 ± 24	95			
Paranaiba (L6/S6) host#1[c]	520–680	5	312 ± 3			750	0.4	11/24
	700–780	5	No trapped	467 ± 6	90			
Mbale (L6/S6) whole rock	480–780	8	No trapped	479 ± 7	75	630	0.5	10/22
Taiban (L5/S6) host[d]	600–840	6	297 ± 1	502 ± 14	45	1750	2.1	24/24
	1270–1500	6	126 ± 5		25			
Bluff (L6/S6) host	820–1290	12	212 ± 37	491 ± 31	75	1320	1.3	24/26
L chondrite weighted mean	Ghubara melt, Paranaiba, Mbale			469.5 ± 4.8 (5.8)[e]				
	Including Taiban, Bluff, Ghubara xenolith			471.1 ± 4.6 (5.7)[e]				
Ordovician meteorites	Darriwilian base			468.1 ± 1.6				
	Biozone base of earliest *E. variabilis /L. variabilis*			467.3 ± 1.6				

[a]Our results show that previous age estimates were veiled by the presence of excess argon, except for the one on Peace River with two matrix samples having partial plateaus consisting of 3 and 4 argon extractions, yielding an age of 450 ± 30 Myr. Peace River is similar to Mbale and Paranaiba with respect to its low abundance of trapped ^{36}Ar (0.6, 0.7, and 1.1 × 10^{-8}ccSTP/g) and the high degassing degree indicated by K-Ar ages as low as 600–750 Myr. This makes certain temperature extractions largely insensitive to excess argon corrections, yielding nearly correct partial plateaus. However, ^{36}Ar contents of >1 × 10^{-8}ccSTP/g (e.g., Chico, Ghubara, Taiban, Bluff) and/or K-Ar ages of >1000 Myr (Wickenburg, Wetherfield, Ghubara, Taiban, Bluff) need a multiple-isochron approach in order to correct apparent ages. Our study demonstrates that this procedure can yield broad age plateaus, if neutron production of ^{38}Ar from Cl can be suppressed satisfactorily (e.g., by applying Cd-shielding and a short irradiation time).

[b]Age values are error weighted means, uncertainty includes statistical scatter of plateau extractions and neutron flux error (0.2% for Ghubara, 0.7% for Paranaiba, Bluff, 1.2% for Taiban and Mbale). For Mbale, we also corrected the relative neutron dose by 0.52% (1.0064 instead of 1.0012, the latter applied erroneously due to a print error in Kunz et al. 1997).

[c]For Paranaiba we obtained a plateau age slightly lower than Kunz et al. (1997), because we used the exact isochron intercept slightly higher than air, instead of the normal air value.

[d]Gas extractions of Taiban at intermediate temperatures do not belong to the partial isochrons and are not used to calculate the plateau age.

[e]Error includes NL25 standard uncertainty of 2660 ± 9 Myr, error in brackets includes 0.7% uncertainty of K decay constant (M. Villeneuve in Gradstein et al. 2004).

These consistent results obtained after correction for trapped excess argon strongly suggest a uniform age, i.e., a single large impact event rather than multiple impact events about 500 Myr ago. The weighted average of the individual results from five L chondrites (Table 2) of 471.1 ± 4.6 Myr is indistinguishable from the three most precise samples that yield a value of 469.5 ± 4.8 Myr (Table 2). The errors include the NL25 standard age uncertainty (Schaeffer and Schaeffer 1977). Adding the K decay constant uncertainty of 0.7% (M. Villeneuve in Gradstein et al. 2004) yields an overall error of 5.8 Myr (see Table 2 and the Samples and Experimental Procedures section). This considerably improves previous age estimates based on partial plateaus or single extractions (Heymann 1967; Turner 1969; Bogard et al. 1976, 1995; Bogard and Hirsch 1980; Kaneoka et al. 1988; McConville et al. 1988; Kunz et al. 1997). All in all, we recommend a ^{40}Ar-^{39}Ar date of 470 ± 6 Myr for the L chondrite parent body breakup. Our result also supports the geochronological significance of two Rb-Sr dates for Point of Rocks and Chico (Nakamura et al. 1990; Fujiwara and Nakamura 1992) of 464.0 ± 9.4 Myr (weighted average, without Rb decay constant error).

Apparent ages were calculated using the Steiger and Jäger (1977) conventions. Although these decay constants are currently under revision, we still consider our age value reliable: first, we included a 0.7% uncertainty for the K decay constants (see, e.g., M. Villeneuve in Gradstein et al. 2004). Second, our age value for the NL25 standard of 2.66 Gyr is the upper limit; a concurrently used value is 2.65 Gyr (Bogard et al. 1995). This would cause a 470 Myr age to appear 3.0 Myr younger, while current studies suggest K-Ar ages—using revised decay constants—should be older by about 1% (Kwon et al. 2002, Renne 2000) or less (Trieloff et al. 2001), i.e., 4.7 Myr relative to U-Pb-Pb ages (the latter dominate the Darriwilian base age of 468.1 ± 1.6 Myr in the geological time scale by Gradstein et al. 2004). Hence, these two effects nearly compensate each other.

The above described multiple isochron approach, the identification of different trapped argon components and its correction in ^{40}Ar-^{39}Ar age spectra, clearly shows that highly irregular (uncorrected) age spectra become plateau-like and yield concordant age values, allowing a calculation of the L chondrite parent body event with improved accuracy/precision. However, defining isochrons and plateaus requires selection of data, influencing the outcome. In the Uncertainties Due to Selection of Isochron Data Points, Plateau Extractions, and Averaging Values section of the Appendix, we show that the effects of data selection are minor and do not change the overall results within uncertainties. First, the L-chondrite parent body event value of 470 ± 6 Myr is mainly defined by the precise values of Ghubara melt, Paranaiba, and Mbale. Even taking largely different values for the less precise Bluff and Ghubara xenolith and Taiban samples, the overall result would not change within uncertainties. Nevertheless, these samples demonstrate that the multiple isochron approach yields consistent results, which would not have been the case if no correction for trapped argon was applied. Samples from Mbale and Paranaiba do not have trapped argon in their main extractions that dominate the age information, so their precise plateau ages do not depend on the choice of a specific trapped component. The selection of plateau fractions is also relatively straightforward in the way that extractions within 2–3σ of the plateau value were taken for the plateaus, while extractions differing by more than 3σ were not used. Nevertheless, even omitting or including such individual extractions (as described in the Appendix) does not change the overall results within uncertainties. For Ghubara melt, trapped argon corrections are important, but the isochrons are well defined, and only one extraction could be ambiguous (980 °C). Omitting or including the intermediate temperature extraction (980 °C) to one or the other array does not change the overall results either. Finally, we also considered a possible systematic age difference between low and high temperature extractions—possibly caused by ^{39}Ar recoil redistribution—but here as well the influence on the age results is marginal (see the Appendix).

DATED PHASES, CARRIERS OF RADIOGENIC AND TRAPPED ARGON, MULTIPLE ISOCHRON APPROACH

In K-Ar and ^{40}Ar-^{39}Ar-dating of whole-rock samples, K-bearing phases are carriers of the chronological information. The K-budget of unshocked, metamorphosed ordinary chondrites (petrologic types 4–6) is dominated by Na-rich plagioclase (oligoclase) which releases radiogenic ^{40}Ar and K-derived ^{39}Ar at temperatures between 700 and 900 °C (Trieloff et al. 2003a). Its modal abundance is ~10%, i.e., significantly less abundant than other major minerals like olivine and pyroxene. On the other hand, the Ca budget is dominated by pyroxene, releasing Ca-derived ^{37}Ar at high temperatures of about 1300 °C. In shocked ordinary chondrites, high-pressure modifications of plagioclase occur: maskelynite (isotropic glass of plagioclase composition), melt veins, and/or pockets with feldspathic glass. The high-pressure phases may also have a hollandite structure (Gillet et al. 2000). In ^{40}Ar-^{39}Ar-dating of shocked chondrites containing high-pressure phases, a common characteristic is the presence of release peaks of radiogenic ^{40}Ar and K-derived ^{39}Ar at high temperatures >1100 °C (Bogard et al. 1976; Bogard and Hirsch 1980; Kunz et al. 1997). This observation also applies to Ghubara melt and xenolith samples that have release peaks of K-derived ^{39}Ar at 700–1000 °C (with K/Ca ratios agreeing with EMPA data of mesostasis in Table 1), 1100–1300°C, and >1300 °C. ^{40}Ar-^{39}Ar dating of experimentally shocked plagioclase (Trieloff 1993) suggests that the high temperature release, or

the generally complex release pattern, is characteristic for high-pressure phases like maskelynite or plagioclase melt glass (and/or K-hollandite), but in detail this effect is hardly understood. In Ghubara melt, glass of feldspathic composition shows considerable chemical variation, especially in K and Ca contents. The ^{39}Ar release at high temperatures possibly can be explained by degassing of more refractory Ca-rich glass.

Another unknown concerns the siting of trapped argon: there is hardly any firm identification of the carrier phase of trapped primordial argon, and the release temperature for equilibrated ordinary chondrites seems to be high (>1100 °C). Trapped atmospheric argon is generally released at low temperatures (<900 °C). In some cases this may simply be adsorbed air, in other cases (desert meteorites) it may be bound to alteration phases (Korochantseva et al. 2005). For the Ghubara samples, we observe release peaks of trapped argon at <900 °C, and 1–2 release peaks at >1000 °C.

Our preferred interpretation is that Ghubara (or in general, the shocked L chondrite samples considered here) were affected by the 470 Myr event and lost part of their primordial (partly solar-wind implanted) argon (^{40}Ar/^{36}Ar < 1). Radiogenic ^{40}Ar was completely mobilized by the thermal effects of that event. Only very retentive high temperature phases (olivine, pyroxene, shock phases?) retained or retrapped some primordial argon, along with pre-existing radiogenic argon (^{40}Ar) that equilibrated/mixed with primordial argon. This resulted in a retentively bound, trapped argon component with a ^{40}Ar/^{36}Ar ratio ranging between 120 and 240 (identified by the high temperature isochron). During the subsequent 470 Myr, radiogenic ^{40}Ar accumulated in the K-bearing phases until the meteorite fell onto Earth. Uptake of slightly fractionated atmospheric argon via terrestrial weathering or simple adsorption is capable of producing the low-temperature isochron, if weathering affects primarily K-free phases (as indeed observed: metal/sulfides) and not plagioclase feldspar, and if the meteorite releases no other previously trapped argon component in the low-temperature release regime.

THE DEPOSITIONAL AGE OF FOSSIL METEORITES AND TRANSFER OF L CHONDRITES TO EARTH

Our refined age value can be compared with the stratigraphic age of the mid-Ordovician fossil meteorites. The earliest bed containing fossil meteorites in the Thorsberg quarry in Sweden is the Arkeologen, a local traditional bed name (Schmitz et al. 1997, 2001, 2003). The unit is characterized by disappearance of the conodont *Lenodus antivariabilis* and replacement by *Lenodus variabilis*. This event can be correlated with the lowermost Kundan stage in Baltoscandia (Löfgren 2003; Landing et al. 2003), and corresponds to the lowermost Darriwilian stage in the Ordovician (Landing et al. 2003; Webby 1988). According to the revised Geologic Time Scale 2004 (Gradstein et al. 2004), the base of the lower Darriwilian stage in the mid-Ordovician is at 468.1 ± 1.6 Myr. The earliest appearances of *Lenodus variabilis* in Baltoscandia correlate with the base of biozones containing *Eoplacognathus variabilis* (Löfgren 1985, Rasmussen 1991), which is ~0.8 Myr younger than the Darriwilian base (Gradstein et al. 2004), i.e., 467.3 ± 1.6 Myr.

These age values are in excellent agreement with our L chondrite value of 470 ± 6 Myr, and we can infer that the fall and deposition of fossil meteorites occurred within a few Myr after the L-chondrite parent body breakup. The contemporaneity of these two events is the missing link in establishing a causal relationship, and particularly consistent with the recently demonstrated short transfer time of fossil meteorites (Heck et al. 2004) after their ejection from a larger planetary body. Our results favor ejection directly after disruption from the L chondrite parent body and effective subsequent orbital evolution of the small fragments, most probably via the strong 3:1 or 5:2 Jupiter resonances (Zappala et al. 1998), rather than the possibility that the fossil meteorites resided for a longer time on an intermediate-size L parent-body fragment after the major collision. Ejection during the main collision as small fragments is also consistent with the fact that no fossil meteorites or extraterrestrial chromites were found in sections below the Arkeologen.

The rocks comprising the recent terrestrial L chondrite influx, including Ghubara, either did not leave or reaccreted to larger parent body fragments about 470 Myr ago. They were strongly shocked and heated by the impact. Our results show that the regolith breccia Ghubara received its solar noble gas inventory before the L-chondrite parent event, as solar ^{36}Ar was effectively equilibrated with radiogenic ^{40}Ar mobilized via impact-induced degassing. For most L chondrites, argon degassing was incomplete, but argon equilibration was in some cases possible on a millimeter-to-centimeter scale (indicated by equilibrated trapped components within individual samples). However, equilibration did not take place on a meter scale, as indicated by different trapped argon components with distinct (^{40}Ar/^{36}Ar)$_{trap}$ ratios in different L chondrites (Table 2). These ratios are lower than terrestrial values, proving the extraterrestrial origin from the transient "atmosphere" resulting from the degassing asteroid. However, in some chondrites, inherited ^{40}Ar and trapped argon was not mobilized to equilibrate, precluding isochron dating even if trapped ^{36}Ar was identified properly, e.g., for Walters and Ness County (Kunz et al. 1997).

INCREASED CRATERING RATE FOLLOWING THE L-CHONDRITE PARENT BODY DISRUPTION?

The agreement between terrestrial and extraterrestrial rock ages is the first direct geochronological proof of a causal link between two events on two different planets in our solar

system. It identifies the fossil meteorites indeed as L chondrite fragments that rapidly traveled from the asteroid belt to Earth in the middle Ordovician after a large impact on the L parent asteroid. The consequences of this impact were probably severe for Earth, which may have been targeted by larger projectiles from the asteroid disruption. These have been preserved as fossil meteorites, but were destroyed upon impact and formed craters. Schmitz et al. (2001) already noted the high number of impact craters in the Middle to Late Ordovician (450–480 Myr ago). Our new age value for the L chondrite event of 470 ± 6 Myr serves as a precise time marker to calculate the cratering rate before and afterwards, confirming that the terrestrial impact crater base (*Earth Impact Database 2003*) displays a significantly increased cratering rate by at least a factor of about 4. There are 8 impact structures with ages between 450 and 470 Myr (Neugrund, Granby, Ames: 470 Myr; Kärdla, Tvären, Lockne: 455 Myr; and Slate Islands, Calvin: 450 Myr). Their diameters range from 2 to 30 km, which indicates sufficient impact energy to certainly cause severe environmental effects. Nevertheless, we stress here the importance of getting more precise radiometric ages for these craters to improve causal relationships.

Schmitz et al. (2001) favored the possibility of this enhanced flux being due to the L chondrite asteroid disruption. However, they cautioned that ordinary chondrite material is probably a very minor component in the asteroid belt (Meibom and Clark 1999), as some scientists argue that the high abundance of ordinary chondrites among terrestrial finds (80%) is the result of a strong selection process (mainly impact destruction and weathering of carbonaceous chondrites). This would raise the question if a factor of 10 increase of L-chondrite projectiles could at all be reflected in an enhanced cratering rate, which should be dominated by carbonaceous chondrite asteroids.

However, this view does not contradict the numbers inferred above. First, it has to be noted that the recent estimate of the influx of small meteorites based on extraterrestrial Ordovician chromite is a factor of 100 higher (Schmitz et al. 2003) than the present total meteorite fall rate based on fireball observations (Halliday et al. 1989). As the fireball data may well contain carbonaceous material—in much higher proportions than the meteorite finds—the actual flux increase of ordinary chondritic material can even be much higher than a factor of 100. Even if we assume that the increase of ordinary chondritic material was of a factor of 100, this would cause a factor of 4 higher cratering rate, if the fraction of ordinary chondrite asteroids among the Earth impacting population is only 4%. Although Earth impactors are derived from the asteroid belt, the number of 4% strictly refers to the Earth-approaching Apollo asteroid population, and not to the whole asteroid belt (e.g., there may be selection processes that enhance ordinary chondrite asteroids in this population, probably related to the mechanisms responsible for orbital evolution like impact fragmentation or spatial relation to resonances). A minimum abundance of 4% is not in contradiction with estimates from spectroscopic studies (Binzel et al. 1996) that as many as 6 out of 35 Apollo objects could be ordinary chondrite objects. We emphasize that in this respect it is invalid to use abundance estimates of ordinary chondrite material in the main asteroid belt, or to use the abundance data of interplanetary dust particles. Here, the low value of 1% ordinary chondrite material may just be due to one or more of the following effects: 1) additional contributions, not yet quantifiable, of cometary dust particles; 2) bias of the dust particle population to the more fragile carbonaceous chondrite material, which is more susceptible to space and collisional erosion; and 3) the possibility that interplanetary dust may represent more the main belt than the Apollo asteroid population, as the transport of dust from the asteroid belt to the Earth obeys different forces (Poynting-Robertson) than transport of asteroids (orbital evolution via Jovian and Kronian resonances).

Acknowledgments–We thank Ray Burgess, Ichiro Kaneoka, and Tim Swindle for very constructive reviews that improved the manuscript. We thank the Forschungszentrum Geesthacht (GKSS) for access to neutron irradiation facilities. We acknowledge support by the Deutsche Forschungsgemeinschaft and Klaus Tschira Foundation. C. A. L. and M. A. I. acknowledge financial support by Austria-Russia project RFBR-BSTC (project #14/04 and grant 03-05-20008).

Editorial Handling—Dr. Timothy Swindle

REFERENCES

Alexeev V. A. 1998. Parent bodies of L and H chondrites: Times of catastrophic events. *Meteoritics & Planetary Science* 33:145–152.

Binns R. A. 1968. Cognate xenoliths in chondritic meteorites: Examples in Mezö-Madaras and Ghubara. *Geochimica et Cosmochimica Acta* 32:299–317.

Binzel R. P., Schelte J. B., Burbine T. H., Sunshine J. M. 1996. Spectral properties of near-Earth asteroids: Evidence for sources of ordinary chondrite meteorites. *Science* 273:946–949.

Bogard D. D. and Garrison D. H. 2003. ^{39}Ar-^{40}Ar ages of eucrites and thermal history of asteroid Vesta. *Meteoritics & Planetary Science* 38:669–710.

Bogard D. D., Garrison D. H., Norman M., Scott E. R. D., and Keil K. 1995. ^{39}Ar-^{40}Ar age and petrology of Chico: Large-scale impact melting on the L-chondrite parent body. *Geochimica et Cosmochimica Acta* 59:1383–1399.

Bogard D. D. and Hirsch W. C. 1980. ^{40}Ar/^{39}Ar dating, Ar diffusion properties, and cooling rate determinations of severely shocked chondrites. *Geochimica et Cosmochimica Acta* 44:1667–1682.

Bogard D. D., Husain L., and Wright R. J. 1976. ^{40}Ar-^{39}Ar dating of collisional events in chondrite parent bodies. *Journal of Geophysical Research* 32:5664–5678.

Brereton N. R. 1970. Corrections for interfering isotopes in the ^{40}Ar/^{39}Ar dating method. *Earth and Planetary Science Letters* 8:427–433.

Earth Impact Database. 2003. http://www.unb.ca/passc/ImpactDatabase. Accessed on November 22, 2005.

Ferko T. E., Wang M.-S., Hillegonds D. J., Lipschutz M. E., Hutchison R., Franke L., Scherer P., Schultz L., Benoit P. H., Sears D. W. G., Singhvi A. K., and Bhandari N. 2002. The irradiation history of the Ghubara (L5) regolith breccia. *Meteoritics & Planetary Science* 37:311–327.

Fujiwara T. and Nakamura N. 1992. Additional evidence of a young impact-melting event on the L-chondrite parent body (abstract). 23th Lunar and Planetary Science Conference. pp. 387–388.

Gillet P., Chen M., Dubrovinsky L., and El Goresy A. 2000. Natural $NaAlSi_3O_8$-hollandite in the shocked Sixiangkou meteorite. *Science* 287:1633–1636.

Gradstein F. M., Ogg J. G., and Smith A. G., editors. 2004. *A Geologic Time Scale 2004.* Cambridge: Cambridge University Press. 589 p.

Halliday I., Blackwell A. T., and Griffin A. A. 1989. The flux of meteorites on the earth's surface. *Meteoritics* 24:173–178.

Hayatsu A. and Palmer H. C. 1975. K-Ar isochron study of the Tudor Gabbro, Grenville Province, Ontario. *Earth and Planetary Science Letters* 25:208–212.

Heck P. R., Schmitz B., Baur H., Halliday A. N., and Wieler R. 2004. Fast delivery times of meteorites to Earth after a major asteroid collision. *Nature* 430:323–325.

Heizler M. T. and Harrison T. M. 1988. Multiple trapped argon isotope components revealed by ^{40}Ar/^{39}Ar isochron analysis. *Geochimica et Cosmochimica Acta* 52:1295–1303.

Heymann D. 1967. On the origin of hypersthene chondrites: Ages and shock effects of black chondrites. *Icarus* 6:189–221.

Huneke J. C. and Smith S. P. 1976. The realities of recoil: ^{39}Ar recoil out of small grains and anomalous patterns in ^{39}Ar-^{40}Ar dating. Proceedings, 7th Lunar Science Conference. pp. 1987–2008.

Jessberger E. K., Dominik B., Staudacher Th., and Herzog G. F. 1980. ^{40}Ar-^{39}Ar ages of Allende. *Icarus* 42:380–405.

Kaneoka I., Takaoka N., and Yanai K. 1988. ^{40}Ar-^{39}Ar analyses of Yamato-75097 (L6) chondrite from Antarctica. *Proceedings of the NIPR Symposium on Antarctic Meteorites* 1:206–214.

Korochantseva E. V., Trieloff M., Buikin A. I., Hopp J., and Meyer H. P. 2005. ^{40}Ar/^{39}Ar dating and cosmic-ray exposure time of desert meteorites: Dhofar 300 and Dhofar 007 eucrites and anomalous achondrite NWA 011. *Meteoritics & Planetary Science* 40:1433–1454.

Kunz J., Trieloff M., Bobe K. D., Metzler K., Stöffler D., and Jessberger E. K. 1995. The collisional history of the HED parent body inferred from ^{40}Ar-^{39}Ar ages of eucrites. *Planetary and Space Science* 43:527–543.

Kunz J., Falter M., and Jessberger E. 1997. Shocked meteorites: Argon-40-argon-39 evidence for multiple impacts. *Meteoritics & Planetary Science* 32:647–670.

Kwon J., Min K., Bickel P. J., and Renne P. R. 2002. Statistical methods for jointly estimating the decay constant and the age of a dating standard. *Mathematical Geology* 34:457–474.

Landing E., Westrop S. R., and Kim D. H. 2003. First middle Ordovician biota from southern New Brunswick: Stratigraphic and tectonic implications for the evolution of the Avalon continent. *Canadian Journal of Earth Science* 40:715–730.

Löfgren A. 2003. Conodont faunas with *Lenodus variabilis* in the upper Arenigian to lower Llanvirnian of Sweden. *Acta Palaeontologica Polonica* 48:417–436.

Löfgren A. 1985. Early Ordovician conodont biozonation at Finngrundet, south Bothnian Bay, Sweden. *Bulletin of the Geological Institute of the University of Uppsala* 10:135–148.

McConville P., Kelley S., and Turner G. 1988. Laser probe ^{40}Ar-^{39}Ar studies of the Peace River shocked L6 chondrite. *Geochimica et Cosmochimica Acta* 52:2487–2499.

Meibom A. and Clark B. E. 1999. Evidence for insignificance of ordinary chondritic material in the asteroid belt. *Meteoritics & Planetary Science* 34:7–24.

Nakamura N., Fujiwara T., and Nohda S. 1990. Young asteroid melting event indicated by Rb-Sr dating of the Point of Rocks meteorite. *Nature* 345:51–52.

Pellas P., Fieni C., Trieloff M., and Jessberger E. K. 1997. The cooling history of the Acapulco meteorite as recorded by the ^{244}Pu and ^{40}Ar-^{39}Ar chronometers. *Geochimica et Cosmochimica Acta* 61:3477–3501.

Rasmussen J. A. 1991. Conodont stratigraphy of the Lower Ordovician Huk Formation at Slemmestad, southern Norway. *Norsk Geologisk Tidsskrift* 71:265–288.

Renne P. R. 2000. ^{40}Ar/^{39}Ar age of plagioclase from Acapulco meteorite and the problem of systematic errors in cosmochronology. *Earth and Planetary Science Letters* 175:13–26.

Schaeffer G. A. and Schaeffer O. A. 1977. ^{40}Ar-^{39}Ar ages of lunar rocks. Proceeding, 8th Lunar Science Conference. pp. 2253–2300.

Schmitz B., Häggström Th., and Tassinari M. 2003. Sediment-dispersed extraterrestrial chromite traces a major asteroid disruption event. *Science* 300:961–964.

Schmitz B., Peucker-Ehrenbrink B., Lindström M., and Tassinari M. 1997. Accretion rates of meteorites and cosmic dust in the Early Ordovician. *Science* 278:88–90.

Schmitz B., Tassinari M., and Peucker-Ehrenbrink B. 2001. A rain of ordinary chondritic meteorites in the Early Ordovician. *Earth and Planetary Science Letters* 194:1–15.

Schwarz W. H. and Lippolt H. J. 2002. Coeval argon-40/argon-39 ages of moldavites from the Bohemian and Lusatian strewn fields *Meteoritics & Planetary Science* 37:1757–1763.

Steiger R. H. and Jäger E. 1977. Subcommission on geochronology: Convention on the use of decay constants in geo- and cosmochronology. *Earth and Planetary Science Letters* 36:359–362.

Stöffler D., Keil K., and Scott E. R. D. 1991. Shock metamorphism of ordinary chondrites. *Geochimica et Cosmochimica Acta* 55: 3845–3867.

Trieloff M. 1993. Datierung impaktmetamorpher Gesteine und methodische Ergänzungen zur ^{40}Ar-^{39}Ar Altersbestimmungstechnik. Ph.D. thesis, University of Heidelberg, Heidelberg, Germany.

Trieloff M., Jessberger E. K., and Fiéni C. 2001. Comment on "^{40}Ar/^{39}Ar age of plagioclase from Acapulco meteorite and the problem of systematic errors in cosmochronology" by Paul R. Renne. *Earth and Planetary Science Letters* 190:267–269.

Trieloff M., Reimold W. U., Kunz J., Boer R. H., and Jessberger E. K. 1994. ^{40}Ar-^{39}Ar thermochronology of pseudotachylite at the Ventersdorp Contact Reef, Witwatersrand Basin. *South African Journal of Geology* 97:365–384.

Trieloff M., Weber H. W., Kurat G., Jessberger E. K., and Janicke J. 1997. Noble gases, their carrier phases, and argon chronology of upper mantle rocks from Zabargad Island, Red Sea. *Geochimica et Cosmochimica Acta* 61:5065–5088.

Trieloff M., Deutsch A., and Jessberger E. K. 1998. The age of the Kara impact structure, Russia. *Meteoritics & Planetary Science* 33:361–372.

Trieloff M., Jessberger E. K., Herrwerth I., Hopp J., Fiéni C., Ghélis M., Bourot-Denise M., and Pellas P. 2003a. Structure and thermal history of the H-chondrite parent asteroid revealed by thermochronometry. *Nature* 422:502–506.

Trieloff M., Falter M., and Jessberger E. K. 2003b The distribution of mantle and atmospheric argon in oceanic basalt glasses. *Geochimica et Cosmochimica Acta* 67:1229–1245.

Turner G. 1971. ^{40}Ar-^{39}Ar dating: The optimization of irradiation parameters. *Earth and Planetary Science Letters* 10:227–234.

Turner G. 1969. Thermal histories of meteorites by the ^{39}Ar-^{40}Ar method. In *Meteorite research,* edited by Millmann P. Dordrecht: Reidel. pp. 407–417.

Turner G. and Cadogan P. H. 1974. Possible effects of ^{39}Ar recoil in ^{40}Ar-^{39}Ar dating. Proceedings, 5th Lunar Science Conference. pp. 1601–1615.

Webby B. D. 1988. Steps toward a global standard for Ordovician stratigraphy. *Newsletters in Stratigraphy* 36:1–33.

Zappala V., Cellino A., Gladman B. J., Manley S., and Migliorini F. 1998. Note: Asteroid showers on Earth after family breakup events. *Icarus* 134:176–179.

APPENDIX

Construct Proper Isochrons for Dating Meteorites: Deconvoluting Trapped, Cosmogenic, and Neutron-Induced Components

An important point how to construct isochrons should be stressed here: trapped argon with distinct $^{40}Ar/^{36}Ar$ ratios (and a unique $^{36}Ar/^{38}Ar$ ratio of 5.35) was obviously incorporated by L chondrites 470 Myr ago. Afterwards, the meteorites analyzed here were still part of a larger parent body (or a large remnant of it). A few tens of million years ago, these meteorites were ejected by smaller impacts into space as meter-size bodies and exposed to cosmic rays. This led to production of cosmogenic argon (primarily ^{38}Ar and ^{36}Ar with $^{36}Ar/^{38}Ar = 0.65$). The decomposition of trapped and cosmogenic argon is performed by determining the $^{36}Ar/^{38}Ar$ ratio (between 0.65 and 5.35) and is only reliable if an additional ^{38}Ar component from Cl (reactor-induced via $^{37}Cl(n,\gamma\beta^-)^{38}Ar$) is not present in significant quantities, lowering the $^{36}Ar/^{38}Ar$ ratio below 0.65. We note here that using total ^{36}Ar to construct isochrons is doubtful, as it violates a basic principle of the isochron approach: isochron dating assumes the presence of i) a single trapped component with a distinct $^{40}Ar/^{36}Ar$ ratio (e.g., by equilibration of pre-existing radiogenic and trapped argon during total reset at time zero, e.g., 470 Myr ago, or admixing of a purely trapped—non-K-related—component later), and ii) another single radiogenic (K-related) ^{40}Ar component. However, cosmogenic ^{36}Ar is mainly produced in Ca phases like pyroxene during the last tens of Myr. This means that cosmogenic ^{36}Ar (with $^{40}Ar/^{36}Ar << 1$) released at high temperatures from pyroxene would interfere with the high-temperature ^{36}Ar and ^{40}Ar trapped 470 Myr ago. As these cosmogenic and trapped components would be released in similar temperature regimes (but not in identical proportions in each temperature step), the use of total ^{36}Ar would fail to construct isochrons, as it is an invalid approach ab initio.

Uncertainties Due to Selection of Isochron Data Points, Plateau Extractions, and Averaging Values

The multiple isochron approach presented in this paper implies the identification of different trapped argon components and its correction resulting in plateau-like (instead of highly irregular) ^{40}Ar-^{39}Ar age spectra that improves the age value of the L chondrite parent body event. Here we discuss the effect of data selection on the result and precision of isochron and plateau age values as well as the average result.

As shown in Table 2, the final average value of the L-chondrite parent body event is largely dominated by the precise age data of Ghubara melt, Paranaiba, and Mbale. Indeed, the less precise Taiban, Bluff, and Ghubara xenolith values are consistent, but they change the average value only by +1.6 Myr, i.e., insignificant within uncertainties. Taking alternative values, e.g., the age values of the partial plateaus of Taiban (low temperature extractions [519 ± 12 Myr] or high temperature extractions [433 ± 25 Myr], instead of the total age of 502 ± 14 Myr), the average age of all samples will change to 473.3 Myr or 468.4, respectively, i.e., indistinguishable within uncertainties. Similarly, alternative values for Bluff and the Ghubara xenolith will not change the overall result, due to the relatively high uncertainties of these results. Nevertheless, these samples are basically very useful for demonstrating that the multiple isochron approach readily turns irregular into plateau-like age spectra, and that the results are in better agreement with more precise samples.

So the actual critical point to be discussed is the evaluation of the precise plateau ages of Ghubara melt, Paranaiba, and Mbale.

For Mbale, which has no detectable trapped argon component, the plateau age does not depend on a correction of trapped argon, but only on selection of plateau extractions. In the case of Mbale, the selection is quite straightforward: we selected extractions for the plateau that did not differ by more than 2σ from the plateau value (in most cases also individual neighboring extractions agree within their 2σ errors). A critical point here may be if we include the 820 and 870 °C extractions; however, their apparent ages of 520 ± 3 and 529 ± 3 Myr differ by more than 8σ from the plateau value and also from the preceding 780 °C extraction with 480 ± 2 Myr, so we consider their inclusion unjustifiable. Nevertheless, we note that even the inclusion of these extractions would not change the average result: the Mbale age would become 485 ± 10 Myr, but this higher and less precise age value would not change the weighted average of Ghubara melt, Paranaiba, and Mbale significantly (468.9 ± 5.0 instead of 469.5 ± 4.8 Myr).

For Paranaiba, we argue similarly that the ages of the high temperature extractions (700–780 °C) are independent of the composition of the trapped component. Moreover, these ages dominate the total age (plateau value using these fractions only: 466 ± 8 Myr, instead of 467 ± 6 Myr), as the

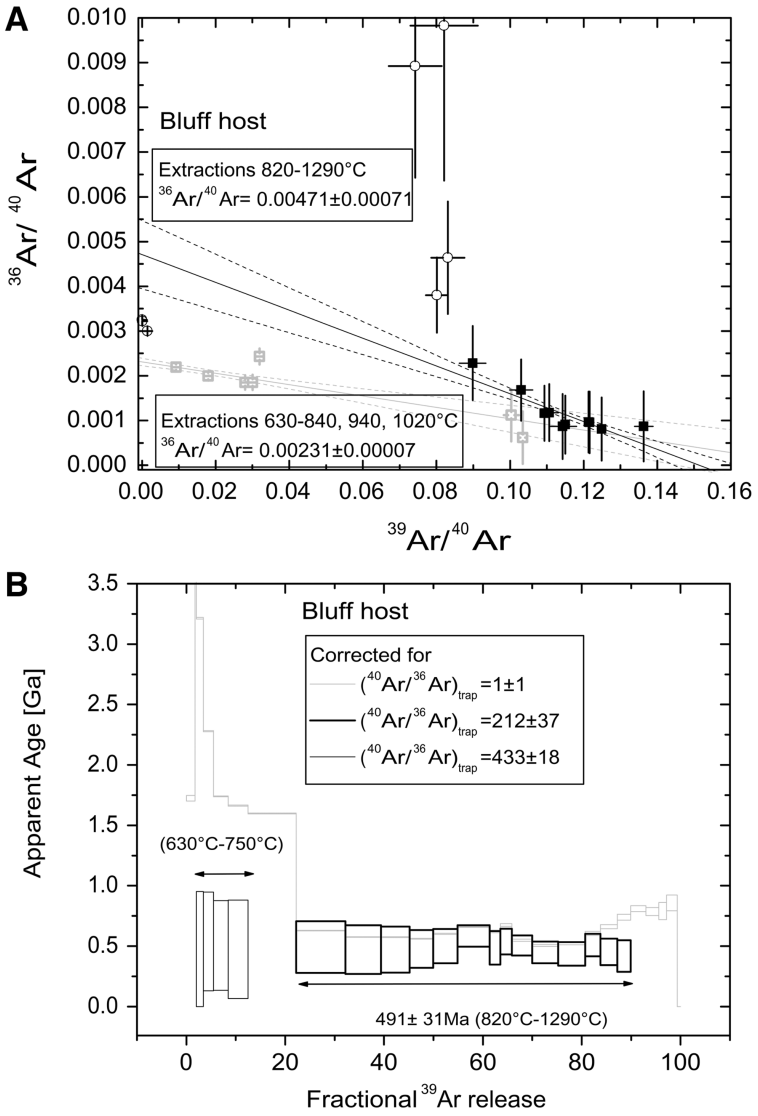

Fig. A1. a) Isochron plot for L6 chondrite Bluff. Two arrays are also recognizable, though not as well defined as in the cases of Ghubara and Taiban. b) The age spectrum for Bluff, similar to that for the Ghubara xenolith, consists of segments with large uncertainties. However, the age value of 491±31 Myr agrees well with our result of 470 ± 6 Myr of the L chondrite breakup event.

low-temperature ages corrected for the trapped component have rather large uncertainties, so all in all the total age does not depend too much on the isotopic composition of the trapped argon. The plateau selection criteria for Paranaiba are similar to Mbale, as the ages of individual plateau extractions agree with the plateau value or the neighboring steps within 2σ mostly. The extractions after the plateau with apparent ages of 548 ± 6 Myr and 535 ± 11 Myr differ by more than 8σ and 5σ, respectively, and accordingly were not included. It may be argued that 700 °C and 780 °C extractions should not be included as they agree only within 3σ with their neighboring extractions, but their exclusion would result in a plateau value of 457 ± 5 Myr (instead of 467 ± 6 Myr), changing the average to 464.3 ± 4.5 Myr (instead of 469.5 ± 4.8 Myr), i.e., still insignificant. However, we think removing the intermediate 700 °C extraction with the "correct" age of 488 Myr seems quite doubtful. If we only remove the last fraction (780 °C), the plateau age would become 465.7 ± 6.5 Myr for Paranaiba and the average would be 469.1 ± 4.9 Myr as average, i.e., as well indistinguishable from the result shown in Table 2.

Finally, we consider Ghubara melt. Here, the correction for the trapped component is highly important and essential for the result. Although the partial isochrons are well defined by two distinct arrays of data points with small uncertainties, the crucial point here is if the 980 °C extraction between the two arrays is included or excluded. While in the main text we prefer to exclude the 980°C extraction as the transitional extraction between the two trapped components, we here consider the case if it was included. We would obtain slightly

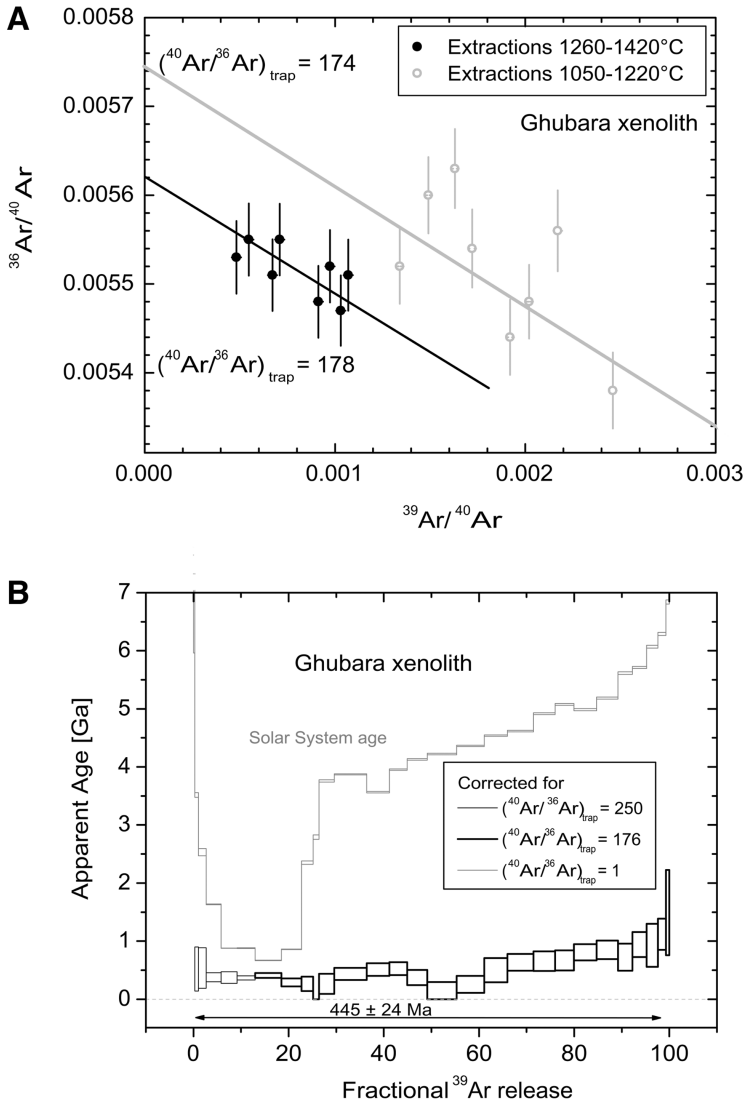

Fig. A2. a) Isochron plot for the Ghubara xenolith. Medium-to-high temperature extractions line fit is dominated by 1050–1420 °C extractions that form a tight cluster. This tight cluster may be furthermore subdivided into two arrays that slightly differ in their $(^{40}Ar/^{36}Ar)_{trapped}$ ratio of 174 and 178, respectively (see Table A2). b) Correction of the age spectrum with an average value of $(^{40}Ar/^{36}Ar)_{trapped}$ = 176 results in a less well-defined age spectrum when compared with Fig. 3b, where the age spectrum is corrected with 174 (1050–1220 °C) and 178 (1240–1420 °C). However, note that the "plateau" age is indistinguishable (445 ± 24 Myr).

different trapped components of $^{40}Ar/^{36}Ar$ = 307.3 for the low-temperature array and $^{40}Ar/^{36}Ar$ = 231.9 for the high-temperature array (instead of $^{40}Ar/^{36}Ar$ = 303 and $^{40}Ar/^{36}Ar$ = 235.8). Moreover, the high-temperature array (980–1560 °C) can be divided in two groups. If we leave out the less-precise 1320–1560 °C extractions, the correlation coefficient of the remaining 980–1260 °C extractions is 0.99615 (instead of 0.99526 for the 980–1560 °C), which would shift the value of the trapped component to $^{40}Ar/^{36}Ar$ = 226.1. Correcting the age spectrum using these trapped argon components yields partial plateau ages of 482 ± 10 Myr (730–980 °C; $^{40}Ar/^{36}Ar$ = 307.3) and 452 ± 7 Myr (980–1560 °C; $^{40}Ar/^{36}Ar$ = 226.1), with a total age of 468 ± 6 Myr instead of 465 ± 6 Myr. Using this value would change the average age of Ghubara melt, Mbale, and Paranaiba by +1.2 Myr, i.e., again insignificantly.

An additional point might be considered here: the partial plateaus defined by low and high temperature extractions of Ghubara melt slightly differ in age, with 482 ± 10 Myr (730–980 C°; $^{40}Ar/^{36}Ar$ = 307.3) and 452 ± 7 Myr (980–1560 C°; $^{40}Ar/^{36}Ar$ = 226.1). Although this is only marginally significant (2σ) in this case, using alternative trapped components appear to make the difference more significant: 491 ± 7 Myr (730–940°; $^{40}Ar/^{36}Ar$ = 303) and 435 ± 5 Myr (1020–1560 °C; $^{40}Ar/^{36}Ar$ = 235.8). Similarly, the corrected Paranaiba low temperature plateau extractions—if taken together as partial plateau—yield 515 ± 13 Myr and seem to

differ slightly in age from the subsequent partial plateau of 466 ± 8 Myr. While this also is only marginally significant, a more compelling observation can be made for Taiban, where low- and high-temperature age plateaus are 519 ± 12 Myr and 433 ± 25 Myr, respectively. For the Ghubara xenolith, Bluff, and Mbale we did not observe possible systematic differences in low and high temperature ages.

In cases where this systematic difference is significant (Taiban, Paranaiba), we might consider two possible explanations: first, slight effects induced by ^{39}Ar recoil redistribution could cause low apparent ages at higher extraction temperatures. However, such a redistribution would still yield the same total age if it occurred within the plateau extractions. The latter seems a reasonable assumption, particularly if plateau fractions constitute a large percentage of the total ^{39}Ar released, as indeed is the case for Ghubara melt and Paranaiba. Hence, we regard this effect to have no significant change in our overall results. Second, we may consider that data selection for isochrons—probably further complicated by insufficient deconvolution of chlorine-induced, cosmogenic and trapped ^{38}Ar—resulted in slightly incorrect determinations of trapped components, which could be the case for Taiban where not all data points were taken for isochron calculations. However, for the Ghubara melt sample, we have already shown that using possible alternative trapped components does not support a significant systematic age difference between low and high temperature extractions.

Appendix Tables

Appendix tables display measured argon isotopes corrected for mass discrimination, sensitivity, system blanks, ^{39}Ar and ^{37}Ar decay, relative neutron doses, and interfering isotopes produced on K and Ca during irradiation. Remaining argon isotopes are given in ccSTP/g and have the following composition:

$$^{36}Ar = {}^{36}Ar_{atm} + {}^{36}Ar_{trap} + {}^{36}Ar_{cos}$$

$$^{37}Ar = {}^{37}Ar_{Ca}$$

$$^{38}Ar = {}^{38}Ar_{atm} + {}^{36}Ar_{trap} + {}^{36}Ar_{cos} + {}^{38}Ar_{Cl}$$

$$^{39}Ar = {}^{39}Ar_{K}$$

$$^{40}Ar = {}^{40}Ar_{rad} + {}^{40}Ar_{atm} + {}^{40}Ar_{trap}$$

where *atm* = terrestrial atmospheric argon, *trap* = trapped extraterrestrial argon, *cos* = cosmogenic argon, *Ca* = argon derived from Ca, *Cl* = argon derived from Cl, *K* = argon derived from K, and *rad* = in situ radiogenic argon.

In a few cases (Ghubara melt, xenolith), apparent ages and ^{40}Ar concentrations in tables are given as "uncorrected" and "corrected," i.e., calculated excluding and including the trapped ^{40}Ar components identified in 3-isotope plots. Corrected ages for extractions used to calculate plateau/average ages are marked with an asterisk.

Table A1. ^{40}Ar-^{39}Ar data of Ghubara melt.

Temp (°C)	^{36}Ar (10^{-11})	^{37}Ar (10^{-11})	^{38}Ar (10^{-12})	^{39}Ar (10^{-11})	^{40}Ar (10^{-9})	Uncorrected age (Myr)	Corrected age (Myr)	
$(^{40}Ar/^{36}Ar)_{trap}$ = 303 ± 4								
350	118 ± 3	0 ± 0	209 ± 7	0 ± 0	0 ± 0	0 ± 0		
500	933 ± 17	37 ± 5	1789 ± 33	10 ± 1	0 ± 0	9794 ± 151		
600	2215 ± 41	153 ± 5	4441 ± 82	132 ± 3	0 ± 0	6707 ± 16		
650	226 ± 5	111 ± 8	631 ± 14	234 ± 5	120 ± 10	2305 ± 7		
690	183 ± 4	159 ± 6	530 ± 12	394 ± 8	170 ± 10	1571 ± 3		
730	220 ± 5	134 ± 7	549 ± 13	417 ± 8	150 ± 20	1658 ± 4	457 ± 41	*
770	349 ± 7	155 ± 8	850 ± 18	584 ± 11	210 ± 20	1773 ± 5	450 ± 37	*
810	112 ± 3	212 ± 9	469 ± 11	805 ± 16	330 ± 10	855 ± 2	509 ± 12	*
850	65 ± 2	314 ± 9	514 ± 13	1291 ± 25	520 ± 10	598.1 ± 1.4	508 ± 6	*
900	76 ± 2	387 ± 10	622 ± 14	1539 ± 30	600 ± 10	577.2 ± 1.3	493 ± 5	*
940	77 ± 2	420 ± 12	679 ± 15	1545 ± 30	580 ± 10	553.2 ± 1.1	473 ± 6	*
$(^{40}Ar/^{36}Ar)_{trap}$ = 235.8 ± 1.7								
980	87 ± 2	394 ± 11	653 ± 14	1336 ± 27	494 ± 11	564.8 ± 1.3		
1020	95 ± 3	353 ± 12	631 ± 14	1087 ± 23	367 ± 10	577.2 ± 1.8	433 ± 6	*
1060	77 ± 3	242 ± 9	434 ± 11	736 ± 17	252 ± 9	628.5 ± 1.7	438 ± 10	*
1090	91 ± 3	284 ± 9	472 ± 12	744 ± 17	263 ± 9	677.8 ± 1.9	450 ± 10	*
1130	191 ± 3	599 ± 14	884 ± 19	1205 ± 23	419 ± 12	750.6 ± 2.1	444 ± 8	*
1170	243 ± 5	736 ± 15	988 ± 20	1332 ± 25	462 ± 13	809.8 ± 1.9	443 ± 9	*
1200	629 ± 12	1465 ± 29	2063 ± 39	2339 ± 41	748 ± 23	968 ± 2	412 ± 10	*
1220	585 ± 11	1214 ± 25	1697 ± 32	1399 ± 25	443 ± 18	1234 ± 3	409 ± 14	*
1240	476 ± 9	946 ± 20	1237 ± 25	666 ± 12	215 ± 17	1676 ± 4	415 ± 28	*
1260	423 ± 9	1053 ± 22	1069 ± 22	397 ± 8	123 ± 15	2074 ± 5	400 ± 42	*
1280	384 ± 9	1116 ± 24	939 ± 21	250 ± 5	98 ± 14	2539 ± 10	493 ± 63	*

Table A1. *Continued.* ^{40}Ar-^{39}Ar data of Ghubara melt.

Temp (°C)	^{36}Ar (10^{-11})	^{37}Ar (10^{-11})	^{38}Ar (10^{-12})	^{39}Ar (10^{-11})	^{40}Ar (10^{-9})	Uncorrected age (Myr)	Corrected age (Myr)	
1320	429 ± 10	1700 ± 38	1092 ± 27	274 ± 6	106 ± 20	2552 ± 8	488 ± 81	*
1360	591 ± 15	2650 ± 61	1467 ± 35	201 ± 5	88 ± 25	3415 ± 9	544 ± 132	*
1400	689 ± 19	3594 ± 89	1774 ± 48	270 ± 7	106 ± 35	3196 ± 10	493 ± 142	*
1440	595 ± 26	2411 ± 88	1504 ± 61	270 ± 10	111 ± 51	3000 ± 9	515 ± 206	*
1480	1237 ± 37	5020 ± 130	3120 ± 89	671 ± 18	257 ± 68	2759 ± 7	484 ± 112	*
1520	2043 ± 67	6850 ± 200	5080 ± 160	919 ± 27	390 ± 110	3020 ± 7	526 ± 125	*
1560	1712 ± 82	4680 ± 190	4120 ± 190	637 ± 26	290 ± 150	3298 ± 8	557 ± 253	*
1600	727 ± 95	2160 ± 230	1820 ± 220	311 ± 33	15 ± 15	2987 ± 10		
1660	81 ± 81	620 ± 620	330 ± 330	87 ± 87	0 ± 0	500		
Total	15,960 ± 180	40,170 ± 750	42,660 ± 500	22,080 ± 140		1761		

Table A2. ^{40}Ar-^{39}Ar data of the Ghubara xenolith.

Temp (°C)	^{36}Ar (10^{-11})	^{37}Ar (10^{-11})	^{38}Ar (10^{-12})	^{39}Ar (10^{-11})	^{40}Ar (10^{-9})	Uncorrected age (Myr)	Corrected age (Myr)	
$(^{40}Ar/^{36}Ar)_{trap}$ = 250 ± 10								
450	78 ± 3	9 ± 8	195 ± 11	1 ± 1	159 ± 4	9959 ± 1498		
550	136 ± 4	11 ± 6	358 ± 12	12 ± 5	310 ± 8	6676 ± 706		
600	56 ± 1	8 ± 6	127 ± 6	38 ± 1	149 ± 4	3521 ± 37	796 ± 402	*
650	56 ± 3	0 ± 0	147 ± 9	78 ± 4	156 ± 4	2536 ± 60	674 ± 336	*
700	55 ± 2	14 ± 2	201 ± 7	152 ± 4	146 ± 4	1637 ± 7	448 ± 97	*
750	23 ± 1	34 ± 12	140 ± 14	162 ± 4	67 ± 2	880 ± 3	396 ± 98	*
800	25 ± 1	31 ± 7	131 ± 5	183 ± 5	75 ± 2	882 ± 6		
$(^{40}Ar/^{36}Ar)_{trap}$ = 174								
850	35 ± 2	37 ± 4	272 ± 18	268 ± 8	78 ± 2	669 ± 5	410 ± 42	*
900	53 ± 2	42 ± 6	363 ± 17	205 ± 5	82 ± 2	863 ± 4	296 ± 67	*
950	145 ± 4	43 ± 10	740 ± 21	117 ± 4	206 ± 5	2358 ± 27	309 ± 118	*
1000	119 ± 5	39 ± 4	585 ± 28	61 ± 3	148 ± 5	2797 ± 36		
1050	421 ± 11	53 ± 6	1130 ± 31	154 ± 4	711 ± 17	3767 ± 17	382 ± 160	*
1090	915 ± 23	96 ± 4	2029 ± 51	329 ± 8	1627 ± 40	3878 ± 3	549 ± 96	*
1120	523 ± 13	99 ± 4	1212 ± 32	231 ± 6	939 ± 23	3572 ± 10	601 ± 102	*
1140	531 ± 14	119 ± 8	1270 ± 32	180 ± 5	938 ± 23	3961 ± 8	640 ± 103	*
1160	697 ± 18	144 ± 17	1851 ± 46	204 ± 5	1186 ± 29	4137 ± 12	511 ± 118	*
1180	1108 ± 28	301 ± 8	3018 ± 75	300 ± 8	1843 ± 45	4230 ± 9	314 ± 134	*
1200	1105 ± 28	335 ± 27	2852 ± 71	280 ± 7	1870 ± 46	4369 ± 6	427 ± 131	*
1220	1004 ± 25	267 ± 10	2326 ± 61	236 ± 6	1756 ± 43	4546 ± 5	664 ± 187	*
$(^{40}Ar/^{36}Ar)_{trap}$ = 178								
1240	1155 ± 29	401 ± 11	2509 ± 63	263 ± 7	2058 ± 51	4626 ± 10	459 ± 160	*
1260	1148 ± 29	286 ± 8	2385 ± 60	220 ± 6	2052 ± 50	4925 ± 10	446 ± 190	*
1280	1100 ± 28	175 ± 5	2257 ± 56	191 ± 5	1964 ± 48	5086 ± 11	436 ± 200	*
1300	1244 ± 32	67 ± 49	2547 ± 63	231 ± 6	2244 ± 55	4994 ± 14	609 ± 158	*
1320	1332 ± 34	182 ± 11	2728 ± 68	219 ± 6	2399 ± 59	5195 ± 15	629 ± 183	*
1340	1142 ± 29	172 ± 24	2326 ± 58	144 ± 4	2030 ± 50	5624 ± 20	407 ± 280	*
1360	1211 ± 31	144 ± 9	2484 ± 62	145 ± 4	2166 ± 53	5723 ± 14	646 ± 255	*
1390	1177 ± 30	129 ± 9	2398 ± 63	115 ± 3	2095 ± 51	6078 ± 22	556 ± 459	*
1420	959 ± 24	88 ± 36	1956 ± 49	83 ± 2	1712 ± 42	6298 ± 23	740 ± 333	*
1475	1537 ± 14	49	1087	34	962 ± 24	6848 ± 34		
Total	18,090 ± 110	3376	41,620	4836	32,130 ± 190	4350		

Table A3. ^{40}Ar-^{39}Ar data of the Taiban host.

Temp (°C)	^{36}Ar (10^{-11})	^{37}Ar (10^{-11})	^{38}Ar (10^{-12})	^{39}Ar (10^{-11})	^{40}Ar (10^{-9})	Corrected age (Myr)
$(^{40}Ar/^{36}Ar)_{trap}$ = 297 ± 1						
400	8716 ± 39	183 ± 16	1632 ± 7	40 ± 1	220 ± 200	2246 ± 1150
480	4288 ± 20	141 ± 11	791 ± 5	76 ± 1	20 ± 20	185 ± 701

Table A3. *Continued.* ^{40}Ar-^{39}Ar data of the Taiban host.

Temp (°C)	^{36}Ar (10^{-11})	^{37}Ar (10^{-11})	^{38}Ar (10^{-12})	^{39}Ar (10^{-11})	^{40}Ar (10^{-9})	Corrected age (Myr)	
540	1445 ± 8	68 ± 12	283 ± 4	127 ± 1	90 ± 70	481 ± 341	
600	1115 ± 7	71 ± 11	239 ± 5	374 ± 1	250 ± 80	467 ± 127	*
660	878 ± 7	50 ± 13	276 ± 12	1208 ± 3	890 ± 130	511 ± 66	*
720	447 ± 6	43 ± 17	233 ± 16	1759 ± 4	1320 ± 110	519 ± 37	*
760	310 ± 4	44 ± 11	245 ± 21	2253 ± 5	1660 ± 90	510 ± 24	*
800	214 ± 4	49 ± 12	221 ± 19	2125 ± 6	1600 ± 70	522 ± 19	*
840	184 ± 3	25 ± 17	210 ± 17	1851 ± 5	1400 ± 50	523 ± 17	*
880	148 ± 3	35 ± 7	168 ± 11	1210 ± 3	930 ± 40	530 ± 19	
920	137 ± 3	29 ± 11	152 ± 7	694 ± 2	530 ± 30	531 ± 22	
970	211 ± 3	55 ± 9	269 ± 5	445 ± 1	400 ± 20	603 ± 32	
1030	168 ± 3	43 ± 11	218 ± 4	303 ± 1	300 ± 20	652 ± 40	
1100	111 ± 4	52 ± 9	127 ± 5	455 ± 2	310 ± 20	478 ± 31	
1180	279 ± 7	101 ± 13	271 ± 10	976 ± 3	540 ± 50	397 ± 30	
1230	344 ± 7	154 ± 11	294 ± 9	788 ± 2	370 ± 50	342 ± 41	
$(^{40}Ar/^{36}Ar)_{trap}$ = 126 ± 5							
1270	207 ± 7	93 ± 7	166 ± 6	341 ± 2	259 ± 23	525 ± 41	*
1300	343 ± 9	147 ± 10	261 ± 7	373 ± 2	212 ± 31	407 ± 53	*
1350	641 ± 12	254 ± 13	427 ± 10	659 ± 3	369 ± 47	401 ± 46	*
1400	1084 ± 17	377 ± 19	681 ± 13	989 ± 4	542 ± 69	393 ± 45	*
1450	1542 ± 24	396 ± 24	895 ± 17	1201 ± 4	676 ± 100	403 ± 53	*
1500	820 ± 54	156 ± 50	402 ± 31	463 ± 9	260 ± 190	405 ± 260	*
1530	96 ± 42	31 ± 31	34 ± 24	40 ± 7	38 ± 38	641 ± 2262	
1531	42 ± 42	4 ± 4	6 ± 6	12 ± 7	8 ± 8	461 ± 6350	
Total	23,770 ± 99	2601 ± 84	8501 ± 65	18,760 ± 19			

Table A4. Corrected ages for Paranaiba light host.

Temp (°C)	^{36}Ar (10^{-11})	^{37}Ar (10^{-11})	^{38}Ar (10^{-12})	^{39}Ar (10^{-11})	^{40}Ar (10^{-9})	Age (Myr)	
$(^{40}Ar/^{36}Ar)_{trap}$ = 312 ± 3							
300	84 ± 3	1 ± 1	21 ± 3	2 ± 1	0 ± 0	134 ± 13652	
380	848 ± 7	15 ± 6	173 ± 6	12 ± 1	10 ± 10	553 ± 5276	
450	451 ± 11	16 ± 5	106 ± 4	63 ± 1	51 ± 51	555 ± 657	
520	329 ± 10	69 ± 3	137 ± 6	490 ± 3	319 ± 61	459 ± 78	*
570	319 ± 10	128 ± 9	179 ± 16	1128 ± 9	740 ± 110	460 ± 59	*
610	486 ± 13	254 ± 7	352 ± 22	2249 ± 13	1660 ± 120	512 ± 32	*
650	540 ± 13	309 ± 13	432 ± 29	3087 ± 18	2270 ± 140	511 ± 28	*
680	272 ± 10	321 ± 7	405 ± 31	3246 ± 19	2469 ± 88	525 ± 16	*
700	163 ± 9	255 ± 9	284 ± 28	2616 ± 16	1828 ± 8	488 ± 3	*
720	108 ± 6	216 ± 6	269 ± 21	2226 ± 13	1449 ± 8	458 ± 3	*
740	102 ± 6	191 ± 5	238 ± 19	1999 ± 12	1284 ± 8	453 ± 3	*
760	83 ± 4	149 ± 6	206 ± 15	1556 ± 10	1010 ± 8	457 ± 4	*
780	69 ± 4	126 ± 9	173 ± 12	1246 ± 8	859 ± 8	482 ± 5	*
810	69 ± 5	119 ± 6	146 ± 11	872 ± 6	696 ± 8	548 ± 6	
840	42 ± 5	85 ± 5	89 ± 6	469 ± 4	364 ± 9	535 ± 11	
880	67 ± 5	114 ± 5	114 ± 7	296 ± 2	294 ± 9	660 ± 17	
920	91 ± 5	165 ± 6	148 ± 5	159 ± 2	262 ± 10	992 ± 28	
970	176 ± 7	245 ± 11	276 ± 7	109 ± 1	359 ± 11	1621 ± 33	
1040	355 ± 10	428 ± 9	550 ± 8	104 ± 1	429 ± 12	1877 ± 34	
1120	269 ± 12	442 ± 10	394 ± 7	73 ± 2	190 ± 55	1387 ± 281	
1200	293 ± 12	763 ± 15	410 ± 7	72 ± 1	79 ± 57	722 ± 427	
1300	742 ± 22	1992 ± 35	885 ± 13	83 ± 2	0 ± 0		
1400	1701 ± 44	4637 ± 78	2057 ± 28	183 ± 2	0 ± 0		
1530	2269 ± 65	4511 ± 76	2523 ± 37	204 ± 5	0 ± 0		
1531	0 ± 0	13 ± 6	0 ± 0	0 ± 0	0 ± 0		
Total	9925 ± 91	15,560 ± 120	10,566 ± 86	22,545 ± 42	16,630 ± 260		

Table A5. Uncorrected ages and ^{40}Ar-^{39}Ar data for Mbale.

Temp (°C)	^{36}Ar (10^{-11})	^{37}Ar (10^{-11})	^{38}Ar (10^{-12})	^{39}Ar (10^{-11})	^{40}Ar (10^{-9})	Age (Myr)	
300	11 ± 5	0 ± 0	4 ± 3	0 ± 0	44 ± 6	7226 ± 3041	
360	21 ± 3	0 ± 0	13 ± 2	5 ± 1	66 ± 6	3513 ± 190	
420	32 ± 3	6 ± 1	36 ± 2	47 ± 1	107 ± 7	1282 ± 58	
480	35 ± 3	36 ± 1	97 ± 5	331 ± 2	224 ± 7	486 ± 13	*
530	58 ± 5	98 ± 2	175 ± 14	948 ± 5	605 ± 7	462 ± 5	*
580	103 ± 4	199 ± 3	331 ± 30	2070 ± 10	1411 ± 7	490 ± 3	*
620	180 ± 5	334 ± 4	521 ± 52	3562 ± 13	2387 ± 7	482 ± 2	*
660	210 ± 5	365 ± 4	567 ± 56	3886 ± 14	2563 ± 8	475 ± 2	*
700	216 ± 6	363 ± 4	559 ± 53	3712 ± 13	2439 ± 8	474 ± 2	*
740	229 ± 5	350 ± 4	553 ± 49	3393 ± 12	2266 ± 8	481 ± 2	*
780	230 ± 5	330 ± 4	538 ± 42	2875 ± 10	1918 ± 8	480 ± 2	*
820	227 ± 5	269 ± 3	486 ± 30	2090 ± 8	1528 ± 8	520 ± 3	
870	251 ± 5	256 ± 3	485 ± 26	1743 ± 6	1300 ± 8	529 ± 3	
920	253 ± 6	231 ± 3	411 ± 14	921 ± 3	880 ± 8	654 ± 5	
990	423 ± 11	356 ± 6	556 ± 10	504 ± 6	1330 ± 9	1427 ± 14	
1060	831 ± 19	741 ± 12	1044 ± 17	508 ± 3	2070 ± 10	1896 ± 9	
1140	1054 ± 24	1152 ± 19	1434 ± 18	360 ± 2	1554 ± 12	1966 ± 12	
1220	968 ± 23	1683 ± 27	1427 ± 18	214 ± 2	597 ± 14	1484 ± 25	
1310	1343 ± 32	2955 ± 47	2229 ± 27	123 ± 1	420 ± 19	1697 ± 51	
1400	1907 ± 45	3963 ± 64	2711 ± 33	150 ± 2	504 ± 26	1679 ± 58	
1530	3127 ± 72	4145 ± 67	3341 ± 40	191 ± 3	728 ± 48	1820 ± 78	
1531	69 ± 16	5 ± 5	47 ± 5	0 ± 0	60 ± 45		
Total	11,780 ± 100	17,840 ± 110	17,570 ± 140	27,635 ± 33	24,998 ± 82		